Chapter 7
Electrical Properties

J.C. Fothergill

7.1 Charge Storage and Transport in Polymers and Nanocomposites

7.1.1 Introduction

Wintle (1983) points out that although there are plenty of theories regarding charge transport and storage in polymeric insulation, very little can actually be proved about what is occurring.

In metals, at least under current density conditions that are not too high, we observe "Ohmic" behavior; i.e., the current through the metal is proportional to the voltage across it. It obeys Ohm's law. In semiconductors, things can get more complicated, although it is usually still possible to explain what is going on. If "good" (i.e., non-blocking and non-rectifying) contacts are made to a crystalline semiconductor, then Ohmic behavior is observed. The charge carriers drift (i.e., "conduct") through the semiconductor under the influence of the electric field, E and result in a current density, J:

$$J = \sigma E \tag{7.1}$$

where σ is the conductivity and is given by:

$$\sigma = ne\mu_n + pe\mu_p \tag{7.2}$$

where n and p are the concentrations of electrons and holes, e is the elementary charge of a proton (1.602×10^{-19} C) and μ_n and μ_p are the mobilities of the electrons and holes. Generally either electrons or holes dominate, depending on whether the semiconductor is doped with donors or acceptors.

If a p-n junction exists, however, a non-linear relationship is observed between the current and the applied voltage; this gives rise to the use of such junctions as rectifiers. The higher concentration of electrons in the n-type material causes them

J.C. Fothergill (✉)
University of Leicester, Leicester, UK
e-mail: John.Fothergill@leicester.ac.uk

J.K. Nelson (ed.), *Dielectric Polymer Nanocomposites*,
DOI 10.1007/978-1-4419-1591-7_7,

to diffuse into the p-type material. Similarly, holes diffuse from the p-type to the n-type region. This causes a potential difference between the p and n sides, which causes the charge carriers to drift back to "their own" regions (electrons to the n-type and holes to the p-type). A dynamic equilibrium is achieved in which a contact potential exists between the two sides of the junction and at the junction there is a "depletion" layer in which the concentrations of free electrons and holes are very low. However, since the ionized donor and acceptor atoms cannot move out of the depletion region, they form a space charge, whose polarity and density is equal to that of the dopants. Since the charges either side of the junction must sum to zero, the space charge extends further into the more lightly doped side of the junction.

Under forward bias (i.e. when the p-type semiconductor is more positive than the n-type semiconductor), significant charge carrier movement takes place when the applied voltage approximately exceeds the contact potential. This is due to drift of carriers (i.e., conduction under the electric field) towards the junction where recombination occurs (leading to light emission in the case of an LED). The junction, acting as an interface, is allowing conduction to occur in the semiconductor regions and is controlling the current.

Under reverse bias, the depletion layer, which contains the regions of space charge, widens. Very few holes are available in the n-type region (they will mostly have recombined with the large number of electrons) and so very few holes are injected from the n-type into the p-type region for conduction. Similarly, there are very few electrons injected into the n-type region. The small reverse-bias current flow is mainly due to diffusion of minority carriers to the junction, where they recombine. In this case, the junction is acting to block conduction and the current may reach a saturation value that is not very dependent on the external voltage. Note that, under conditions of either forward or reverse bias, the current is *not* determined directly by the conductivity, as in (7.1). Whilst this is quite complicated, the processes are generally well understood.

7.1.2 Charge Transport in Insulating Systems

The situation in insulators is bound to be even more complicated. Perhaps the simplest scenario to consider would be where the insulator is, in fact, a lightly doped semiconductor (say p^--type) and the electrodes, rather than being metal, are heavily doped semiconductors (say n^+-type), which will behave very much like metals if sufficiently heavily doped. This is shown schematically in Fig. 7.1. In this case, the left p-n junction is forward biased. This could allow current flow and we would expect some electrons to be injected. However, these may recombine with the holes in the p^- type insulator. There is some negative space charge accumulation in the insulation next to the cathode which is known as "homocharge," and this causes a field reduction at this electrode. The right p-n junction is reverse-biased and it would block hole injection, although it may allow electrons to escape from the insulation into the n^+ electrode. A large negative space charge layer forms in the p^- insulator

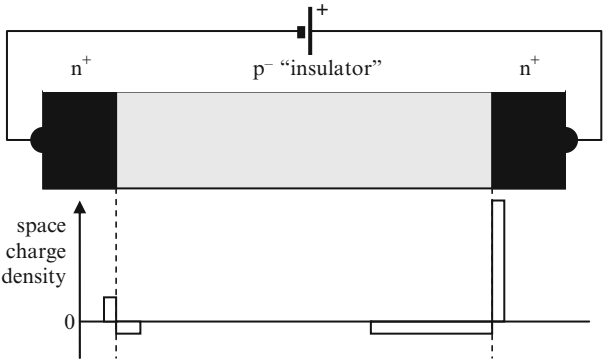

Fig. 7.1 A simple insulating system

adjacent to this positive electrode; which is known as "heterocharge" and this causes field enhancement at this electrode. It can be seen that this is rather like a MOSFET in which no gate voltage is applied and the device is turned off. The behavior of this device is well understood, but it does rely on materials and interfaces that are well characterized both chemically and physically. In particular, it is necessary to understand the nature of the interfaces and whether they will support injection, ejection and recombination under given bias conditions and to understand the nature and processes of transport of charge carriers through the material.

7.1.3 Charge Transport in Polymers

In polymeric insulation, the situation is much less well characterized and less well understood. Some polymeric materials are partially crystalline; perhaps the best known is polyethylene. With its repeating backbone of ethylene units, $-(CH_2) - (CH_2) - etc$, the unit cell is shown in Fig. 7.2, having a height of 255 pm.

These chains fold back and forth to form ribbon-like lamella which may be 50 unit cells thick and thousands of chains wide in the other two dimensions. A "corner" of one of these lamellar is shown schematically in Fig. 7.3. These lamellae are attached to each other by "cilia" – polymer chains that weave from one lamella to another. Further discussion of the physics and chemistry of polymers may be found in Chap. 4.

Within such crystalline parts of polymers, a reasonable electron energy band structure will exist and it would be possible for charges to move through delocalized bands. In polyethylene, the band gap is very wide, approximately 8 eV, and the conduction band edge is above the vacuum level which implies that electrons will be ejected from crystalline regions into the amorphous regions (or electrodes) adjacent to them. However, it may be possible for holes to move through such amorphous

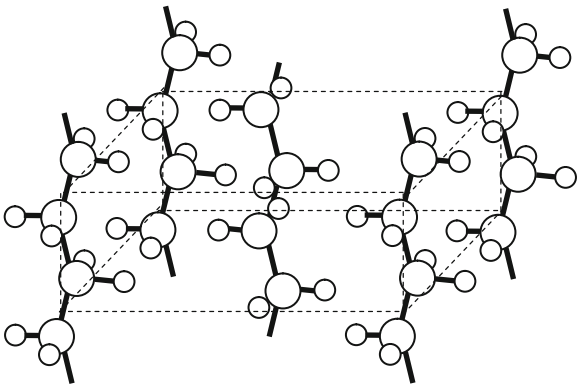

Fig. 7.2 The unit cell of polyethylene (Peacock (2000))

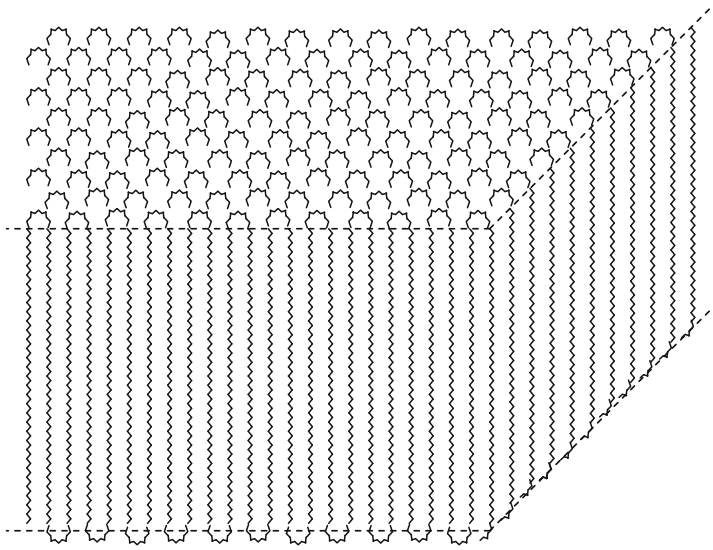

Fig. 7.3 Schematic of a "corner" of a somewhat idealized lamella

regions in polyethylene. Trapping would be likely since the crystalline regions are unlikely to be perfect and, in any case, the charge carrier would never be far from the surface of the lamella where trapping would be inevitable.

Surrounding these crystallites are amorphous regions. In polyethylene this is quite "liquid like" and ionic transport is more likely in these regions. These regions are also likely to contain impurities and additives, which may be polarizable and may even be able to move themselves through the amorphous regions. In these amorphous regions and in wholly amorphous materials (such as epoxy resin), there are likely to be high concentrations of traps.

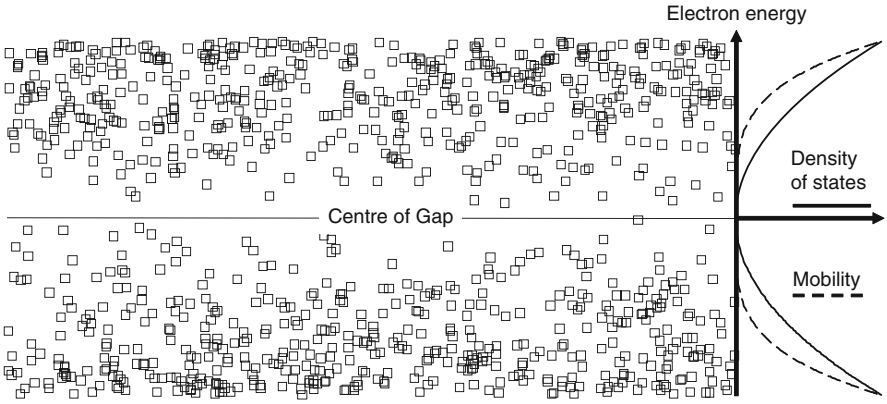

Fig. 7.4 Localized states in a non-crystalline material (indicated by *squares*) as a function of electron energy; the density of states and mobility are also shown (adapted from Dissado and Fothergill 1992)

As one moves from crystalline to amorphous, the well-defined delocalized band structure starts to become interrupted by traps. Eventually, one would expect the traps to dominate, as shown in Fig. 7.4. There is still some semblance of a band structure, but there are fewer traps at energies corresponding to the centre of the gap and there are high trap densities where there were bands. Carriers may be able to hop or tunnel between traps that are physically close to each other and so this results in a "mobility gap" (Mott 1967) near the centre of the band gap where there is a low concentration of states and it is unlikely that hopping or tunneling can take place between them. Conduction through the amorphous regions is therefore likely to be trap limited or ionic (for an overview of these processes see Dissado and Fothergill 1992, Chap. 9). In either case, carriers have to overcome energy barriers to move and so conduction is frequently found to follow an Arrhenius-type relationship:

$$\sigma\,(T) = \sigma_0 \exp\left\{-\frac{U}{kT}\right\} \tag{7.3}$$

where T is the absolute temperature, σ_0 is a constant of proportionality corresponding to a conductivity at 0 K, U is a barrier height and k is the Boltzmann constant (1.381×10^{-23} J K^{-1}). For example, Lampert and Mark (1970) derive the following formula for thermally-assisted ionic-hopping conduction current:

$$J = 2ndv \exp\left\{-\frac{U_B}{kT}\right\} \sinh\left\{\frac{eEd}{2kT}\right\} \tag{7.4}$$

where d is the hopping distance and v is the attempt to hop frequency.

7.1.4 Electrode Effects

Assuming that metal contacts are used, in which the only charge carriers are electrons, "good" contacts must either easily inject/accept electrons into/from the insulation. These electrons might flow through the insulation (perhaps attached to ionized species) or they may recombine with positive carriers (ions or holes).

In an ideal situation in which the metal electrode changes abruptly at a planar surface to become a perfect insulator, then electrons need to overcome a field-dependent Schottky barrier (Dissado and Fothergill 1992), an example is shown in Fig. 7.5. Schottky injection would result in a non-linear relation between current density and field of the form:

$$J \propto \exp\left(\sqrt{E}\right) \tag{7.5}$$

and although this is often observed, the constant of proportionality is usually several orders of magnitude smaller than would be expected. This is probably attributable to chemical and physical defects at the interface on the nanometer scale (e.g., a 2 nm metal oxide layer would result in a decrease of 6–7 orders of magnitude (Lewis 1954).

In practice, electrode – polymer interfaces are unlikely to be "good" even on the nanometer scale, let alone the atomic scale and so it is extremely difficult to predict, in practice, exactly what the effect of electrodes are likely to be – indeed it is thought that electrode effects often lead to irreproducibility in conductivity measurements in polymer insulators.

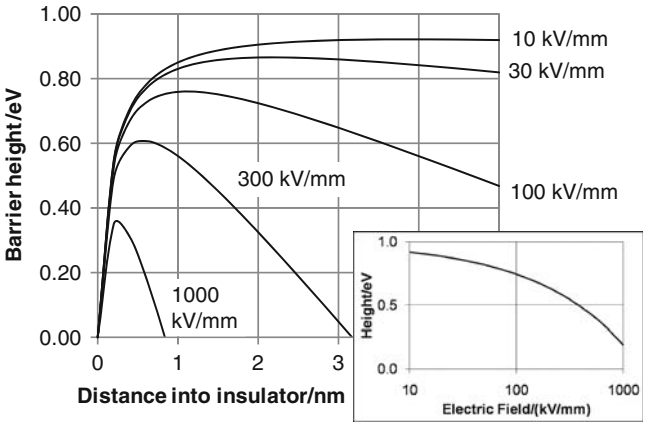

Fig. 7.5 Effective Schottky barrier for a metal with work function = 1 eV and an insulator with a relative permittivity of 2.2 as a function of distance into the insulator plotted for different electric fields. The *inset* shows how the maximum effective barrier height varies with field

7.1.5 Space Charge Effects

Figure 7.6 shows the main behaviors expected of charges in a solid insulator or at the electrodes. Given this variety, Wintle's comments that opened this chapter are not surprising. A further effect of these mechanisms is that charge is not necessarily entering and leaving a region at the same rates. In particular, charge may be injected at an electrode faster or slower than it is transported away in the insulation. Similarly charge may accumulate at an electrode if the coulombic barrier prevents it leaving the insulation as fast as it arrives there. The rate of accumulation will be governed by a continuity equation in which ρ is the total space charge density:

$$\frac{d\rho}{dt} = -\nabla.J \tag{7.6}$$

For example, Fig. 7.7 shows the space charge measurement in crosslinked polyethylene (XLPE) by Teyssedre et al. (2001). It can be seen that positive and negative charge built up on the electrodes as the voltage increased (as one would expect) but also that there was negative charge accumulation near the cathode. A possible reason for this is that electrons were being injected from the cathode corresponding to a current density that was out of balance (i.e., higher than) that due to conduction away from the electrode through the insulation.

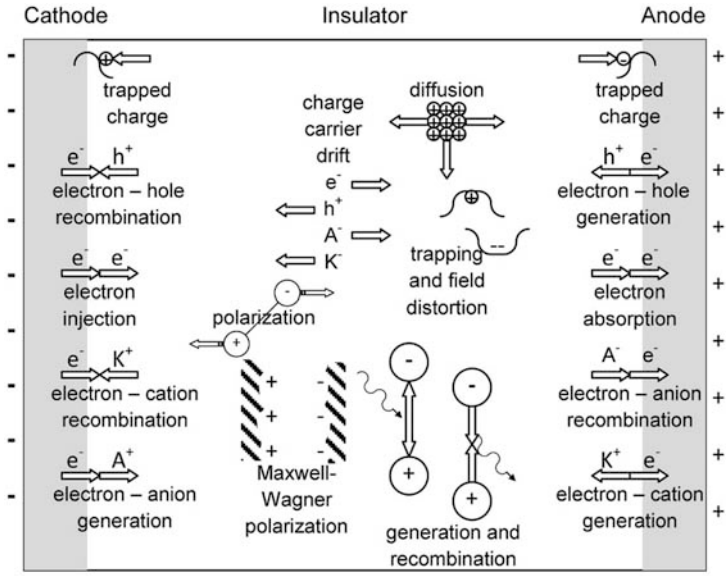

Fig. 7.6 A wide variety of charge behaviors in an insulator or at an insulator – electrode interface affect the external response

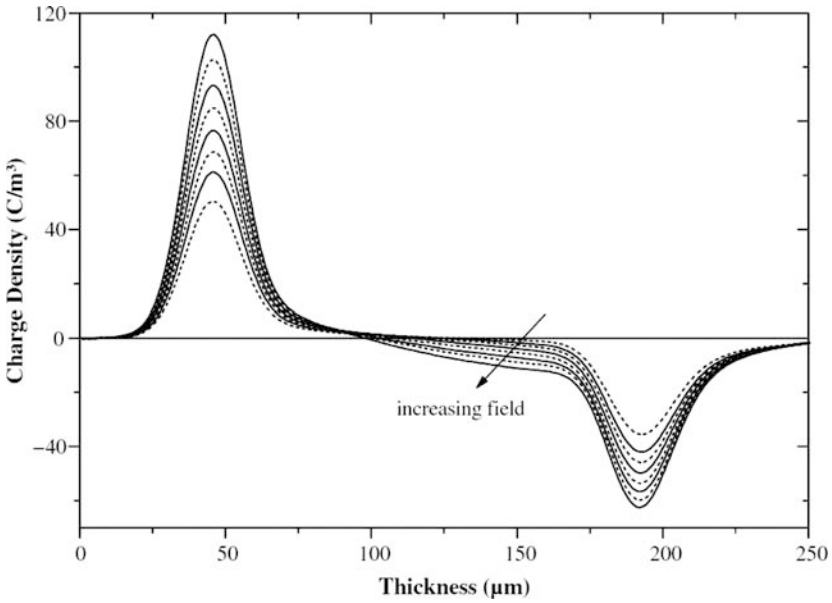

Fig. 7.7 Charge profiles at different fields for a progressive dc stress test on XLPE. The cathode is on the *right* and the anode is on the *left*. Profiles are shown at 60, 72, 80, 88, 96, 104, 112 and 120 kV mm^{-1} (Teyssedre et al. 2001)

The original theory of space charge limited current was developed by Mott and Gurney (1940), in the absence of experimental data from polymeric insulation. They considered an ideal dielectric (no thermal generation of carriers, no traps, ohmic contacts, only electrons, etc.) and showed that above a given voltage, the current would follow a square law. As the charge density builds up it may be expected to fill traps and, if a single trap level is assumed, then this will lead to a very rapid increase in current with voltage. Upon a further increase in voltage (i.e., after the traps are full), the relation of current to voltage would revert to a square law relationship. Given the assumptions in deriving this, it would seem unlikely that this is observed. However, it is commonly observed that, above a given voltage, the current does increase super-Ohmically; often following a square law. Below this voltage, it is often not clear that Ohm's law is obeyed and indeed, considering Fig. 7.1, we might not expect this to be the case. An unusually compliant example is that of Chutia and Barua (1980) shown in Fig. 7.8 for thin films of polyvinylacetate coated with aluminium electrodes.

It can be difficult however, to separate this behavior from the hyperbolic sinusoidal behavior predicted for space-charge limited current by (7.4). Assuming room temperature and a hopping distance of 5 nm, then the sinh term, $\left\{\frac{eEd}{2kT}\right\}$, is less than 1 for a value of $E < 10\,\mathrm{kV/mm}$ so that a slope of 1 on a $\log(J)$ versus $\log(E)$ (i.e., Ohmic behavior) would be predicted in this region (since $\sinh(x) \approx x$ for $x < 1$). Similarly, for fields of 10–30 kV/mm this would result in a plot that was close to

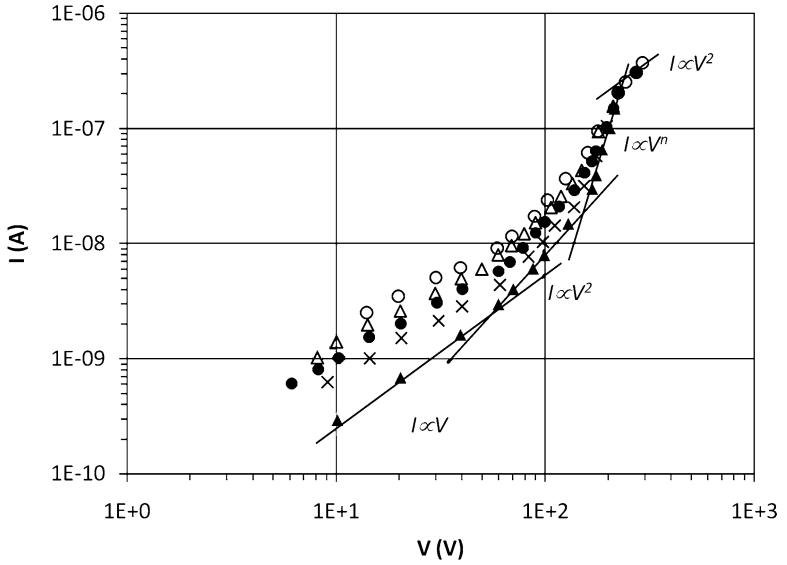

Fig. 7.8 Current–voltage characteristics for 1.2 μm PVAc films at different temperatures: *filled triangle* = −15° C, *times symbol* = 10° C, *filled circle* = 30° C, *open triangle* = 50° C, *open circle* = 80° C (Chutia and Barua 1980)

a straight line with a slope of around 2, perhaps being misconstrued as the onset of SCLC, and above this very high slopes would be observed. Clearly, there would not be a reversion to a slope of 2 at higher fields, but most dielectrics have reached breakdown by this field value.

7.1.6 Effect of Nanoparticles and Interaction Zone on Charge Transport

In considering the effect of the inclusion of nanoparticles (or other inclusions with nanoscopic dimensions) in an insulator there are perhaps two essential factors to take into account: (1) the effect of the nanoparticle on the physical and chemical structure of the material, and (2) how the particle changes the electrical properties of the material surrounding it. The properties of the material surrounding the particle are often substantially changed (certainly from an electrical point of view) and this changed material is said to fall within the "interaction zone" of the nanoparticle. Depending on the concentration and shape and size of the nanoparticles, these interaction zones may overlap giving rise to effects associated with percolation through the interaction zones. The first of these effects has been discussed in detail in Chap. 4. It is noted that surface functionalization of the nanoparticles has a profound effect on the morphology of the insulation and this will at least partly explain the effects on the breakdown voltage noted later in this chapter. Water, oxygen and other

species may also be adsorbed onto the surface of nanoparticles and form a physical layer of a new species between the particle and the host dielectric.

The second of these effects, the change of electrical properties, was explored in a seminal paper by Lewis (1994) entitled "Nanometric Dielectrics" following a theme by the same author that interfaces can dominate observed dielectric behavior. He expanded on this theme in 2004 (Lewis 2004). The "specific area," i.e., the surface area of nanoparticles per unit volume of nanocomposite, is extremely high (see Fig. 1.3) and so his comments are likely to be particularly apposite. Even for spherical nanoparticles, which have the smallest ratio of surface to volume equal to $3/r$, their radius, the specific area is high. In this case, it is equal to $3\psi/r$ where ψ is the volumetric fraction occupied by nanoparticles. So for $\psi = 0.05$ (say) and $r = 50$ nm, one cubic meter of nanocomposite would give rise to three square kilometers of surface area.

In order to remain within the main scope of this book, we will consider insulating particles in an insulating medium. However, it should be noted that there is a significant body of work on conducting nanoparticles (e.g., the carbon nanotubes considered in Chap. 9, or silver aerosol particles) in insulating media and vice versa. In his discussion, Lewis uses similar terminology to that of a charged particle in an electrolyte. For example, suppose that we have a material that has a positive surface charge. (This may arise as a chemical potential – rather like that existing across the p-n junction – or where there are dangling surface bonds, which we might expect in silica for example.)

Figure 7.9 shows a possible scenario. Let us assume that the surface of the particle is charged positively. This may result in a polarization of the host material in

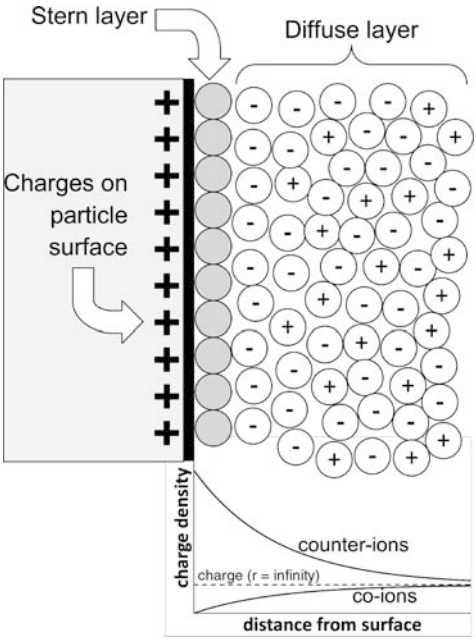

Fig. 7.9 Diffuse double layer produced by nanoparticle with charged surface within a dielectric (adapted from Lewis 2004). On the left is a cross-section through part of the particle showing charges on the surface. On the right is the host polymer

which the particle is located. This process (which is termed "reorganization" in electrochemistry) is dependent upon the permittivity of the medium. A second screening action occurs if the host contains mobile ions. Such ions may include atmospheric molecules that have become ionized by the electric field, for example. A first layer of ions, known as the "Stern" layer (shown as grey circles) may attach to the surface by forces that are stronger than the electrostatic forces attracting the diffusion layer in the interaction zone. In this diffusion layer "co-ions" (i.e., having the same charge as the particle's surface charge) are repelled and counter-ions are attracted towards the particle. Lewis (2004) shows that these may approximate to exponential functions (shown in Fig. 7.9).

The ions in the Stern layer are unlikely to be able to drift under the influence of an electric field. However, the diffuse layer may well be more conductive than the bulk insulation. The preponderance of one type of ion close to the particle implies that these will not be screened and will contribute to the conduction process. Grosse (2006) has considered a similar situation for suspensions of particles in a dielectric liquid. He concludes that, from the dielectric standpoint, a particle surrounded by a surface conductivity, G_S, behaves exactly as if it had no surface conductivity but its bulk (i.e., volume) conductivity were incremented by the $2G_S/a$, where a is the particle radius.

7.1.7 Percolation Effects

Nanoparticles will not be distributed completely uniformly through a nanocomposite. In the absence of forces that cause the particles to be attracted or repelled from one another, there will be a distribution of distances between particles. The implication of this is that interaction zones will overlap to form percolation networks.

Figure 1.2b shows a situation in which a host material is filled with spherical nanoparticles. There are interaction zones shown around each particle. If the widths are equal to the radius of the particle and the loading was 5 wt%, then approximately half the particles will have overlapping interaction zones. Although this is below the percolation level, there would still be significant sub-percolation paths. Furthermore, hopping and tunneling may be possible between zones. An approximation for calculating the probability of overlap (Fothergill 2007) may be undertaken as follows.

Let us assume that we have small spherical particles all of radius, r, that are surrounded by interaction zones of thickness, t. Two such particles will therefore interact if they are separated by a distance $2t$, i.e., if their centers are within a distance $2(r + t)$. This is equivalent to saying that there is more than one particle within a sphere of radius $2(r + t)$. The probability that there are x particles within such a sphere is given by the Poisson distribution:

$$P(x, \mu) = \frac{\exp\{-\mu\}\,\mu^x}{x!} \tag{7.7}$$

where μ is the average number of particles in such a sphere. The probability of two or more particles (the condition for overlap) is therefore[1]:

$$P(x,\mu) \approx 1 - (1+\mu)\exp\{-\mu\} \text{ where } \mu = 8\psi\frac{(r+t)^3}{r^3} \tag{7.8}$$

The "approximately equal" sign is used as the radius of the particle becomes significant for small interaction zone thicknesses and the assumption that the particle is small becomes invalid. An example of this is shown in Fig. 7.10. It can be seen that, for a 5% v/v concentration of 50 nm diameter particles, an interaction zone thickness of 25 nm results in an 83% chance of overlap. This is in qualitative agreement with a 2-D simulation (>75% are interacting). Perhaps a more informative way of considering this is to consider percolation theory (Simulations on granular conductive-insulting composites, which may be useful to this area, have been published by He and Ekere (2004). Balberg (2009) has considered percolation allowing for tunneling between particles.)

The percolation limit for spheres, i.e., the concentration that is normally required to obtain a continuous pathway through touching spheres, p_c, is usually considered to be approximately 19%. An interesting question to ask then is, "What concentration of nanoparticles is required such that their interaction zones form a percolating network?" If there are n nanoparticles per unit volume, then their volumetric concentration, ψ, is obviously:

$$\psi = n \times \frac{4}{3}\pi r^3 \tag{7.9}$$

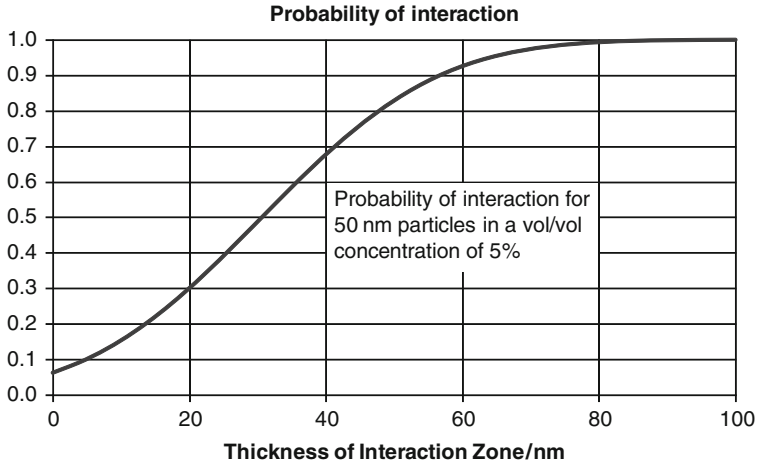

Fig. 7.10 Probability of interaction of the interaction zones of 50 nm spherical particles

[1] Assistance is acknowledged from Prof. Len Dissado with this derivation.

The interaction zones coat the spherical nanoparticles with a layer of thickness, t, so they form spheres of radius $(r + t)$. The volumetric concentration of the interaction zones containing the nanoparticles, ψ_Z, is therefore:

$$\psi_Z = n \times \frac{4}{3}\pi (r + t)^3 \tag{7.10}$$

For percolation to occur, ψ_Z must equal the percolation limit, p_c. The volumetric concentration of nanoparticles required to cause percolation between the interaction zones is therefore:

$$\psi = p_c \frac{r^3}{(r + t)^3} \tag{7.11}$$

Equation (7.11) is slightly oversimplified as it assumes that the interaction zones touch but do not overlap and that will necessarily result in a marked increase in conductivity. However, it should be useful for light loadings of particles. This is shown in Fig. 7.11.

For example, particles with a radius of 15 nm with a 15 nm thick interaction zone would only require a volumetric concentration of 2.4% to reach the percolation limit. *We therefore expect low concentrations of nanoparticles to have significant effects on the electrical properties.*

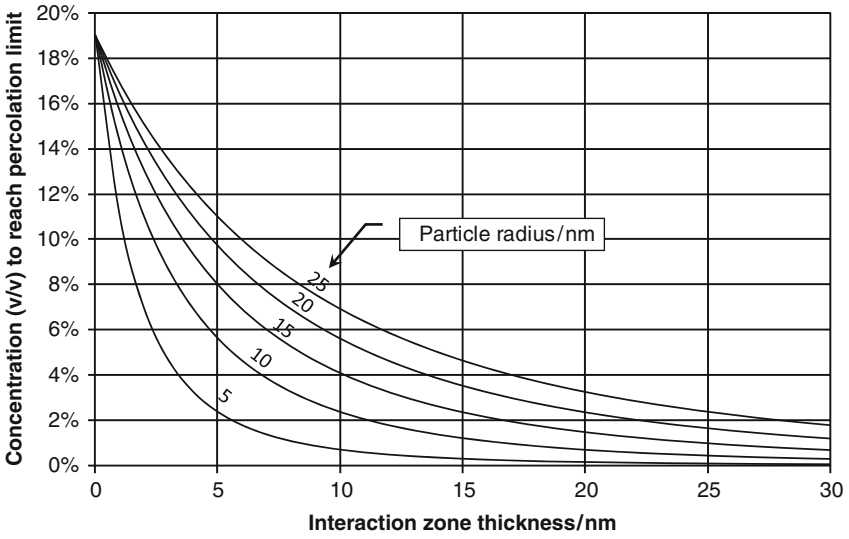

Fig. 7.11 Concentration of nanoparticles required to reach percolation limit from (7.11)

7.1.8 Examples of Charge Movement in Nanocomposites

Cao and Irwin (2003) have investigated the field and temperature dependence of the steady-state current density for a polyimide (PI) polymer with 10 wt% (approximately 6.5 vol%) 40 nm nanoparticles of silica. Their results (more clearly shown in Cao et al. 2004) are reproduced in Fig. 7.12.

Plotting this data on a $\log(J)$ versus $\log(E)$ plot instead would suggest a change from Ohmic to space charge limited current behavior at about 10–20 kV/mm. However, because the temperature dependence here is also found to fit the Lampert and Mark equation (7.4), this may be indicative of an ionic conduction process. The hopping distance is found to be 4.3 nm with activation energy of 0.68 eV. These parameters would not exclude an electronic conduction process, which may give rise to similar behavior. From Fig. 7.11, for percolation to be occurring, this would require an interaction zone thickness of approximately 10 nm. One could imagine a situation in which, for this composite, the interaction zone is less than this, perhaps 5 nm, and ions are required to hop the remaining 5 nm between interaction zones. The same authors reported that a 2 wt% ($\approx$1.6 vol%) addition of nanofiller reduced the conductivity by about half an order of magnitude (at 100°C) whereas an increase to 10 wt% ($\approx$6.5 vol%) increased it from this value by about an order of magnitude. The initial addition of nanofiller may therefore have been causing morphological changes which decreased the conductivity.

Zhang et al. (2006) have found similar results for PI filled with both nano SiO_2 and Al_2O_3. An example of this is shown in Fig. 7.13.

Zhang et al. attribute the change of slopes observed, at least at lower loadings, to the onset of space-charge limited current. This may be true but it would be difficult to be sure without making measurements as a function of temperature as well. For this nanocomposite the wt% and vol% loadings are similar and

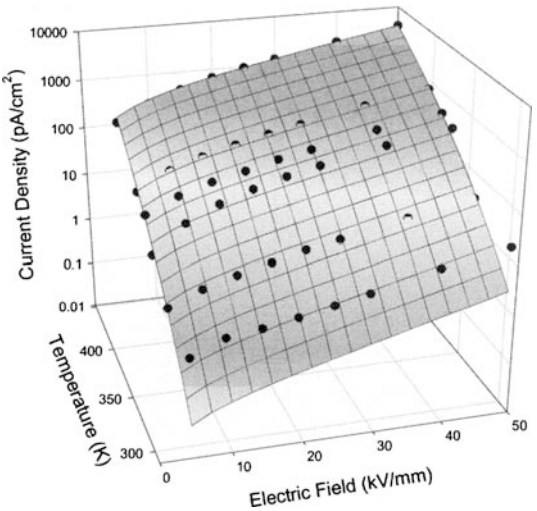

Fig. 7.12 Field and temperature dependence of current density for PI with 10 wt% nano-silica (Cao et al. 2004). © IEEE

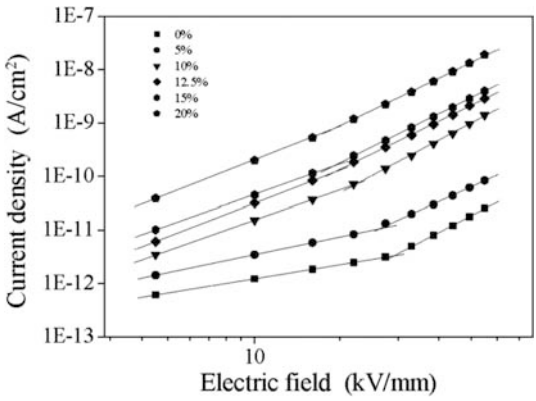

Fig. 7.13 The conduction current in PI filled with nano-Al_2O_3 (Zhang et al. 2006). © IEEE

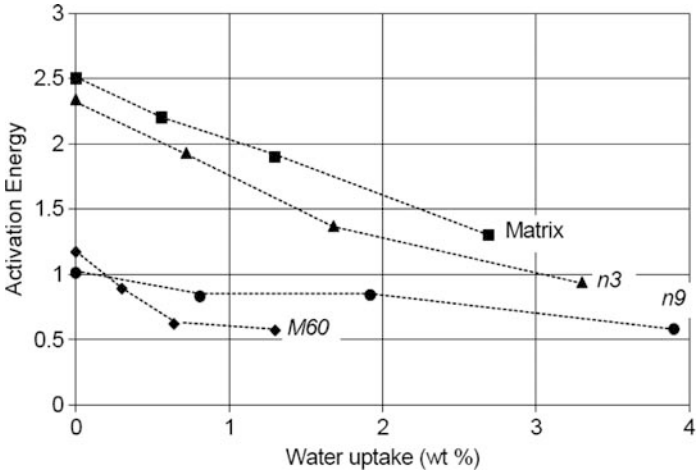

Fig. 7.14 Activation energy in electron-volts of low frequency charge transport process in nano-silica (50 nm diameter) filled epoxy (from Zou et al. 2008). Matrix = unfilled resin, n3 = 3 wt% nanofilled, n9 = 9 wt% nanofilled, M60 = 60 wt% filled with larger silica (tens of microns in diameter)

a substantial change is noted on increasing this from 5 to 10%. It may be that the latter corresponds to transport through substantially overlapping interaction zones. A selection of similar results has been reviewed by Tanaka et al. (2004).

Zou et al. (2008) introduced 50 nm silica particles, without any surface functionalisation, into epoxy resin. It was shown that this introduced a layer of water around the particles (under humid conditions), which we might consider acts as a well-defined interaction zone, whose thickness must be dependent upon humidity. This was also compared with an unfilled epoxy and an epoxy filled conventionally with larger silica particles of tens of microns in diameter. The activation energy of the low frequency charge transport process was found through dielectric spectroscopy at different temperatures. A summary of the results are shown in Fig. 7.14.

The results clearly show that the lightly (3 wt% ≈ 1.5 vol%) nano-filled material behaves very like the unfilled material. The "rate-determining step" in the charge transport is movement between interaction zones through the resin. The interaction zones must be reasonably well separated in this case. However for the more heavily nano-filled material (9 wt% ≈ 4.5 vol%) the activation energy is much lower – suggesting that charge movement is much easier and probably largely through overlapping interaction zones. This is similar to the heavily micro-filled material where we would expect this to be the case. This would suggest interaction zones of around 15–25 nm thick. Although the water layer was not this thick, it is clear from the unfilled material that the charge transport process is influenced by water in the resin itself. It is therefore likely that, although the nanoparticles may have been coated with a few monolayers of water (perhaps corresponding to the Stern layer), there was also a diffuse layer of water extending considerably further into the resin.

7.1.9 Internal Charge Distribution in Nanocomposites

Internal charge that is trapped in an insulating media is known as "space charge" (historically named after the charge that accumulates above the cathode in a thermionic valve). It is generally undesirable since it causes a distortion in the electric field in the insulator. Homocharge (charge near an electrode of the same polarity as the voltage on the electrode) decreases the field near the electrode (which may be desirable) but, because the same voltage is applied across the same thickness and the average field must be maintained, there must be a concomitant increase in electric field elsewhere in the insulation (which is undesirable). Heterocharge increases the field next to the electrode and is almost always undesirable. A reduction in space charge accumulation is therefore an important goal. There is a general increase in the proportion of high-voltage insulators required to support DC voltages as the requirement for long-distance electrical transmission increases. It is therefore particularly important to understand and reduce space charge accumulation in these cases.

Holé et al. (2006) have shown that it is very difficult to measure space charge distributions accurately in nano-filled composites. They analyzed the implications of filler particles on different space charge measurement techniques and showed that they produce perturbations to the space charge distribution signal irrespective of the measurement method. The problem is exacerbated by some particles, such as silica, that exhibit piezoelectricity; these induce a random like signal during the measurement owing to the random distribution and orientation of the particle in the host material. By reverse-engineering the signal they concluded that charge trapping around nanoparticles is likely to occur.

Nelson et al. (2002) were the first to report the reduction of space charge densities through nano-filling composites. Further work by these authors (Nelson and Fothergill 2004) reported how the maximum electric field (caused by the space charge distortion) is reduced by incorporating nanofillers, Fig. 7.15. A voltage of

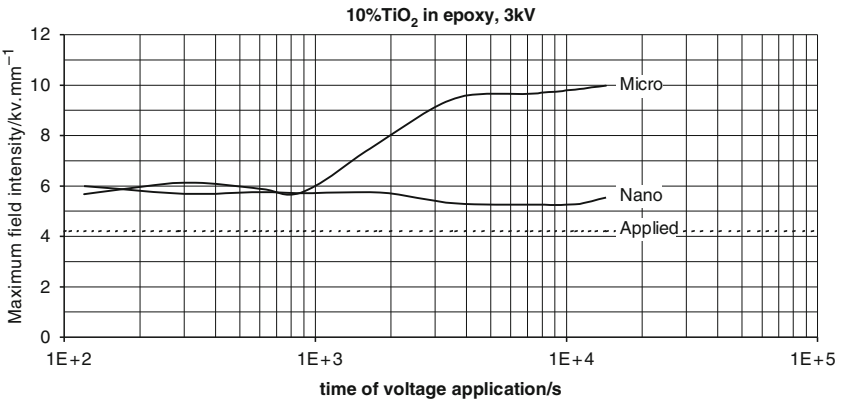

Fig. 7.15 Reduction in field distortion through the incorporation of nanofillers (Nelson and Fothergill 2004)

3 kV was applied to epoxy resin specimens approximately 0.7 mm thick, resulting in an average (or "applied") field of 4.2 kV/mm. The specimens were filled with 10 wt% TiO_2 of either nanometric or micron-sized dimensions. Due to space charge accumulation, the maximum measured field initially was around 6 kV/mm. After about 15 min, the maximum field in the micro-composite increased significantly, as might be expected, as space charge was injected. However, this was not the case in the nanocomposite. In this case, no further space charge injection was observed.

At very high fields, "charge packets" may be observed in some insulators. This is an unstable, chaotic phenomenon in which waves of charge, typically of a magnitude that would double the local field intensity, travel slowly across the insulator. They may take minutes or even an hour to travel a millimeter. Whilst these may not be of particular interest from an engineering point of view – they only happen at very high fields – they may give clues as to the mechanisms of charge transport in such insulators. These charge packets are generally found to be reduced by the addition of nanoparticles. For example, Murata et al. (2008) and Hayase et al. (2007) added nano sized MgO filler to crosslinked polyethylene (XLPE) and reported on the volume resistivity and space charge behavior. The results indicate the suitability of XLPE(S)/MgO nanocomposite material for HVDC insulation; the "S" referring to a "special" XLPE with reduced crosslinking byproducts (This would include acetophenone which is highly mobile and ionizable.) Figure 7.16 shows the charge packet behavior they observed: packets are observed in the XLPE(S) material crossing the specimen in about 20 min. However the nanoparticles appear to quench this behavior completely.

Zilg et al. (2003) have measured space charge accumulation in polypropylene (PP) and ethylene vinyl acetate (EVA) doped with fluorohectorite surface modified with protonated octadecylamin (ODA) in 2, 3 and 6 wt% concentrations. Again they see a general reduction in space charge (Fig. 7.17).

Their conclusions are fairly typical. The magnitude of the space charge decreased at high fields, although this is not necessarily observed at low fields. The space

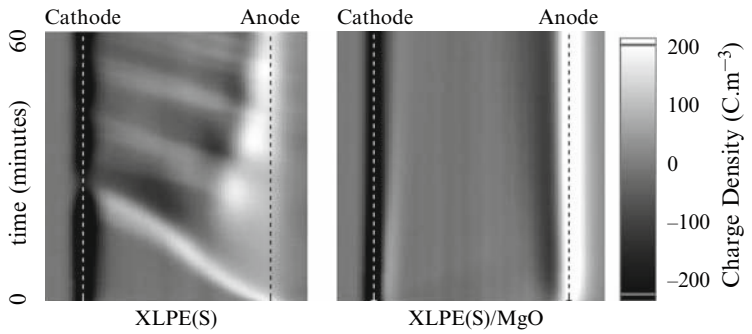

Fig. 7.16 Time dependent space charge distribution in XLPE(S) and XLPE(S)/MgO under electric field of 150 kV/mm (Murata et al. 2008). © IEEE

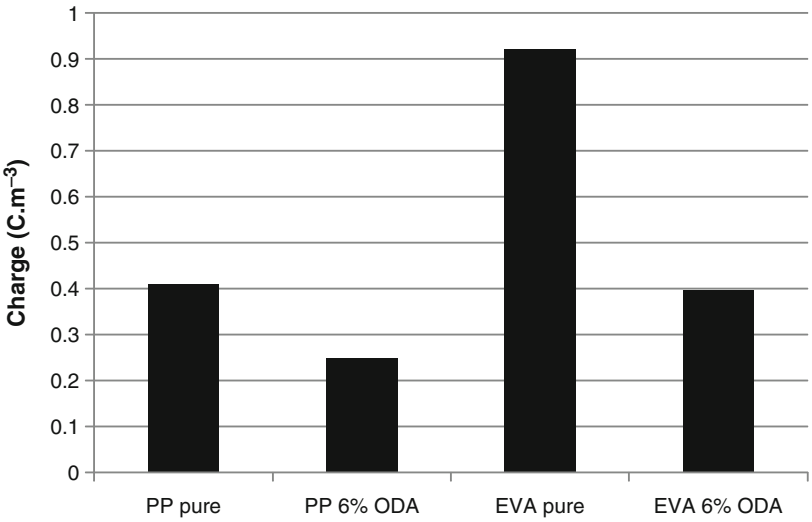

Fig. 7.17 Reduction in space charge observed by Zilg et al. (2003) for PP and EVA doped with fluorohectorite nanoparticles surface modified with protonated octadecylamin (ODA)

charge inception voltage decreased (from 14 to 5 kV/mm for PP) upon the addition of nanofillers – and further decreased if the nanofiller content increased. The decay of charge in the material was faster for the nanofilled materials. The review paper of Tanaka et al. (2004) made similar conclusions. "Nanomization" causes the following effects

- Space charge increases at low fields and decreases at high fields (e.g., Zilg et al. 2003, Ma et al. 2005)
- Space charge inception field decreases (Zilg et al. 2003)
- Space charge is generated internally (Nelson et al. 2002)
- Charge decay time decreases (Zilg et al. 2003; Nelson et al. 2002)

7.1.10 Concluding Remarks on Charges in Nanocomposites

It seems likely that ionic conductivity is enhanced by the addition of nanoparticles to insulating polymers. Small concentrations of particles, surrounded by interaction zones, allow percolation of such ions to be enhanced. Ionic conduction is greatly enhanced by increased electric fields. Space charges can give rise to local increases in electric fields. The increased conduction at these fields by the addition of nanoparticles causes these space charges to disperse. Charges will naturally occur around nanoparticles, increasing the space charge at low fields, however this is at a sufficiently small level that it is unlikely to be a problem at technologically important fields. The space charge inception voltage – i.e., the voltage at which super-Ohmic behavior occurs, may be due to ionic charges. Indeed, it is possible that this onset field is more to do with ionic charge transport than a significant increase in charge accumulation.

7.2 Dielectric Response

7.2.1 Dielectric Spectroscopy

Dielectric spectroscopy is frequently used by engineers to evaluate the effect of using a dielectric in a circuit (be that an electronic circuit or a high voltage transmission system) and by chemists to improve understanding of dipolar processes. Processes include: very low frequency ("sub-Hertz") processes which provide information about charge transport processes; Maxwell-Wagner polarization processes, which provide information about charge trapping associated with internal surfaces (such as those found on nanoparticles and electrodes); and relaxation processes associated with dipoles reorientation.

Dielectric spectroscopy usually involves the application of a sinusoidal voltage and the measurement of the resulting sinusoidal current. The relative amplitudes and phases of the voltage and current allow the complex impedance of the sample to be evaluated. Time domain techniques may also be used and the frequency domain behavior calculated through deconvolution using a Fourier transform. The electrical impedance may be considered as $\mathbf{Z}(\omega) = R(\omega) + \mathbf{j}X(\omega)$ where R is the resistance and X is the reactance of the specimen under test and ω is the angular frequency, i.e., $\omega = 2\pi f$. In order to analyze the loss mechanisms, it is often more convenient to express this impedance as a complex capacitance $\mathbf{C}(\omega) = C'(\omega) - \mathbf{j}C''(\omega) = 1/\mathbf{j}\omega\mathbf{Z}(\omega)$. Measurements are usually made over a range of frequencies and temperatures.

In the case of a capacitive specimen, such as a power cable, the real part of the capacitance, $C'(\omega)$, simply represents the capacitance of the cable, which would normally only change slightly with frequencies around the power frequency. Since this component is reactive, this gives rise to charging ("displacement") currents that are out of phase with voltage under AC conditions but no power loss.

The imaginary part of the capacitance, $C''(\omega)$, is resistive in nature, and therefore does lead to power dissipation. In the case of an XLPE power cable, one would normally expect this to be small and highly frequency dependent. The imaginary part of the capacitance is normally attributed to two types of physical mechanism. Firstly, if there is some sort of DC conduction mechanism that has a conductance, G_{DC}, (i.e., a parallel resistance equal to $1/G_{DC}$), then this will lead to a component of $C''(\omega)$ that is equal to G_{DC}/ω. This is likely to dominate at low frequencies and is easily observable since, on a Bode plot of $\log\{C\}$ versus $\log\{f\}$, C' is flat (slope $= 0$) whereas C'' has a slope of -1. Secondly, there may be power loss due to the movement of dipoles within the dielectric. This is frequency dependent. At sufficiently high frequencies, a given type of dipole will not be able to align quickly enough with the alternating field and so will not dissipate power. At sufficiently low frequencies, the dipole moves so slowly that any power dissipation becomes negligible. There is, therefore, a dispersion or "loss peak" at a frequency at which the maximum power is dissipated. From an engineering point of view, this is equivalent to a frequency dependent conductance, $G_{AC}(\omega)$ so that $C''(\omega) = (G_{DC} + G_{AC}(\omega))/\omega$.

7.2.2 Dielectric Response of Nanocomposites

The addition of nanoparticles causes major changes in the dielectric response consistent with the formation of interaction zones as described earlier. An example, which illustrates these mechanisms, is shown in Fig. 7.18, taken from Nelson and Fothergill (2004).

At high frequencies the micro-composite has a higher relative permittivity, presumably because the filler has a high permittivity ($\approx$99). For example at 1 kHz, the measured real permittivities are: 9.99 (base resin), 13.8 (micro-composite), and 8.49 (nanocomposite). It is interesting that the nanocomposite has a lower permittivity than the base resin. This may be in part due to the very small size of the particles giving rise to limited cooperative movements of dipolar reorientation within them, but it is probably also due to the restriction by the nanoparticles of movement of end-chains or side-chains of the epoxy molecules.

In the mid range of 0.1–100 Hz, the base resin and nanocomposite behave in similar ways; there is some evidence of a small dielectric relaxation possibly due to bound water. The activation energy of this process drops from 1.7 eV for the micro-composite to 1.4 eV for the nanocomposite perhaps indicating that the water is "less bound" – possibly in the diffuse layer around the nanoparticles.

The real permittivity of the micro-composite shows a significant increase with decreasing frequency associated with Maxwell-Wagner interfacial polarization. (Although the frequency for such a mechanism might be considered rather high, the polarization is probably between the micro-particles rather than the electrodes and, as these are quite close together – about 1.5 μm – the time required for polarization to occur is correspondingly small.) The base resin exhibits the classic indicator of Maxwell-Wagner polarization below 0.1 Hz – slopes of -2 and -1 respectively for

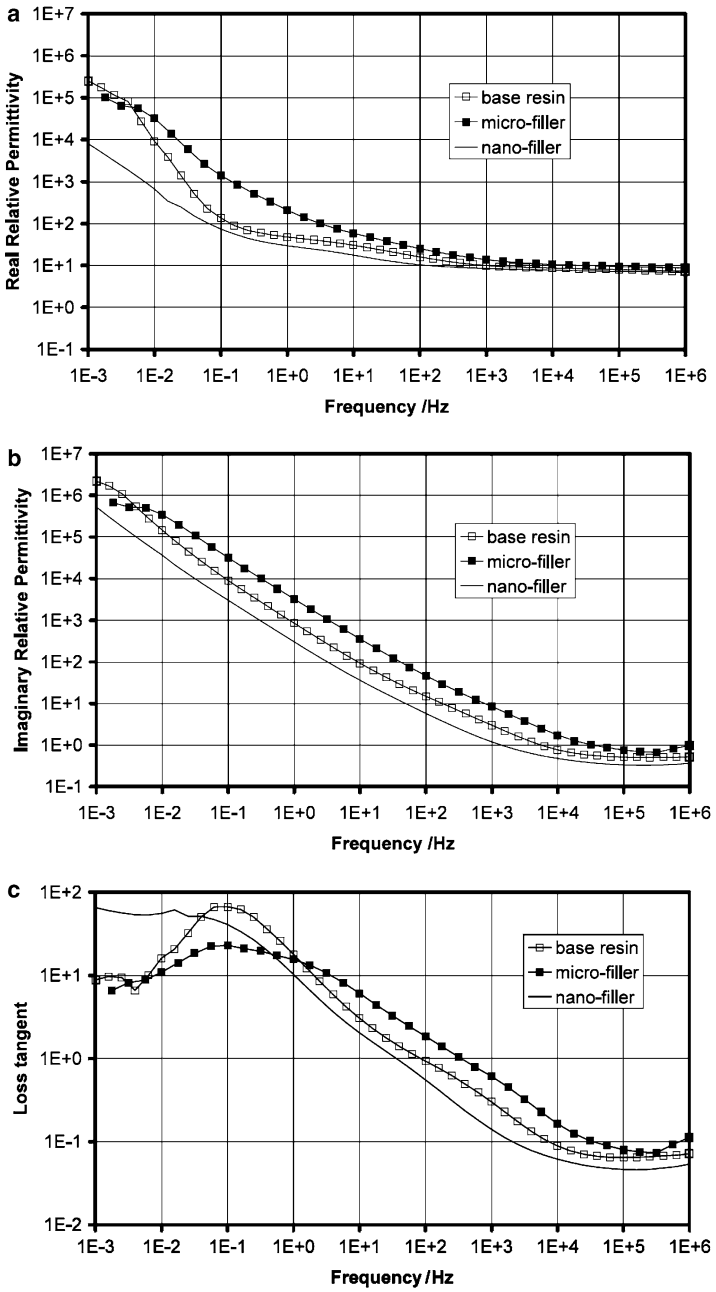

Fig. 7.18 Dielectric response of TiO_2 – epoxy composite (**a**) Real and (**b**) Imaginary parts of permittivity and (**c**) loss tangent (Nelson and Fothergill 2004)

the real and imaginary parts of the permittivity on these Bode plots. This results in a peak in the loss tangent, also observed for the micro-composite – in this case due to Maxwell-Wagner polarization at the electrodes.

The nanocomposite shows quite different behavior at low frequencies. Instead of the real part having a slope of −2, it is parallel to the imaginary part with a slope of −1 and the loss tangent is flat and independent of frequency. This is symptomatic of what Jonscher (1983) refers to as a "low-frequency dispersion" and Dissado and Hill (1984) refer to as "quasi-DC" or QDC. This is characteristic of charge carriers having limited freedom of movement within a material; they may follow tortuous paths that do not allow transport completely through the material. Dissado and Hill (1988) later modeled this in terms of fractal circuits. It seems quite reasonable to assume that such behavior would occur if the paths formed by overlapping interaction zones were at the sub-percolation level for this composite (Although the wt% concentration is 10%, for this combination of particle and host, the vol% concentration is only about 2.8%. So for 38 nm particles, from Fig. 7.11, we might expect to have interaction zones 20 nm thick for percolation to occur.) This transport mechanism is likely to lead to the mitigation of space charge accumulation.

Figure 7.19 shows the dielectric spectroscopy of polyimide measured by Cao and Irwin (2003). The micro-composite has a loss peak at ∼1 kHz, which does not exist for the unfilled material. This corresponds to Maxwell-Wagner interfacial polarization. In the nanocomposite, this interfacial polarization peak is largely reduced by the field mitigation with the shrinking of filler dimension.

Mixing polymers with layered silicates leads to three different types of structures (Elmahdy et al. 2006): phase separated micro-composites; intercalated and exfoliated nanocomposites as discussed in Chap. 3. The dielectric properties of intercalated nanocomposites are markedly different from the base resins. For example Elmahdy et al. (2006) studied the hydrophilic polymer, polyethylene

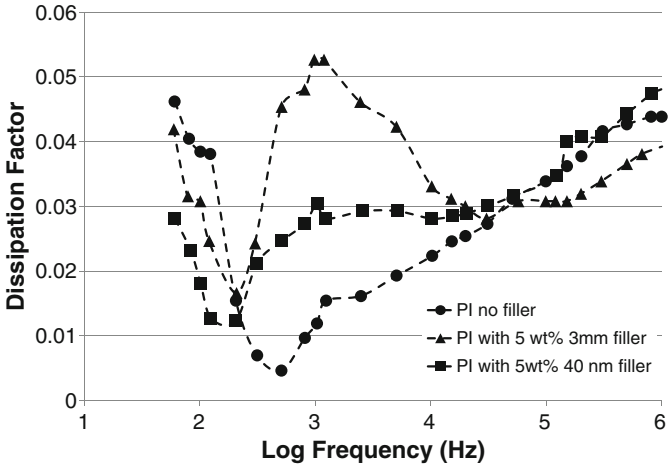

Fig. 7.19 Dielectric dissipation factor for PI nanocomposites (Cao and Irwin 2003)

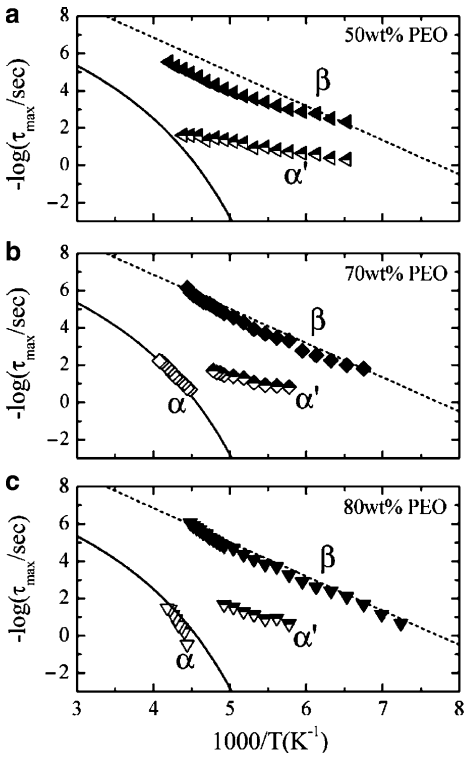

Fig. 7.20 Arrhenius relaxation plots for PEO – Na^+MMT nanocomposites (**a**) 50 wt%, (**b**) 70 wt% and (**c**) 80 wt% PEO (Elmahdy et al. 2006)

oxide (PEO) intercalated within the hydrophilic silicate, sodium montmorillonite, Na^+MMT. These may have applications in electro-active devices and solid-state batteries. The confinement of the PEO films within the MMT galleries causes an increase in the speed of the PEO segmental relaxation (displaying Arrhenius temperature dependence) and also an increased ionic conduction.

Figure 7.20 illustrates this effect, the solid and dashed lines indicating the α and β processes for the pure PEO. The relaxation times of the α-process follow the Vogel-Fulcher-Tamman equation:

$$\tau = \tau_0 \exp\left\{\frac{B}{T - T_0}\right\} \tag{7.12}$$

with $\tau_0 = 1.0 \times 10^{-11}$ s, $B = 2,700 \pm 300$ K and T_0 (the glass transition temperature) $= 112 \pm 10$ K. The relaxation times for the fast local β process of pure PEO correspond to an Arrhenius type process (7.3) with the activation energy $U = 0.36$ eV and $\tau_0 = 6 \times 10^{-15}$ s. For the 50 wt% PEO system (and less), the PEO α process is not observed at all since all the PEO segments are confined within the galleries and relax at a faster rate, shown as an α′ process. In contrast, for the 70 and 80 wt% cases, the α process is seen and is due to the segmental motion of the amorphous regions of the PEO chains that reside outside the galleries and crystallize

in a similar way to that of bulk PEO. The main finding from the dielectric relaxation point of view, is that of a new α' process due to the confinement of polymer mobility. The activation energy of this process is dependent on the PEO concentration: 0.29 eV (80%), 0.18 eV (70%), 0.13 eV (50%) and 0.12 eV (30%). The fast local β-process is observed with a rate comparable to that of bulk PEO due to its local character.

7.3 Electrical Breakdown

7.3.1 Introduction

The increase in reliability of high-voltage products such as power cables (e.g., Bertini 2009) has been largely due to incremental improvements that have reduced contaminants, protrusions (from electrodes) and voids. The effect of new technologies on the electrical breakdown characteristics are therefore difficult to assess. In the case of nanocomposites, one has to compare a mature technology in which virtually perfect electrical insulation systems are compared with insulators that potentially contain agglomerations of particles and impurities and imperfections that are difficult to avoid in a laboratory process. It is therefore unsurprising that there are contradictory results. However, recent results, in which the production processes of nanocomposites have improved, are showing encouraging results.

Electrical breakdown results are frequently analyzed using Weibull statistics and presented on Weibull plots (e.g. IEEE Standard 930 2004) in which the cumulative probability of breakdown (which would equate to the proportion of specimens failed for a large sample size) is plotted on appropriate axes as a function of the breakdown voltage. This is further discussed in Sect. A.9.1 and the probability described by variants of (A.12).

Just as we might expect the charge transport processes to be affected by both changes of morphology and changes to carriers densities and mobilities induced by including nanoparticles, so we would expect these two factors to influence the breakdown characteristics.

7.3.2 Polyethylene Nanocomposites

The effect of morphology is well illustrated by the work of Vaughan et al. (2006) who prepared a range of nanocomposites containing polyethylene and montmorillonite (MMT) clay using different procedures, such that the extent of MMT dispersion varied. They found that when the MMT is poorly dispersed, the short-term breakdown strength is reduced but the situation is much improved when efforts are made to maximize the dispersion.

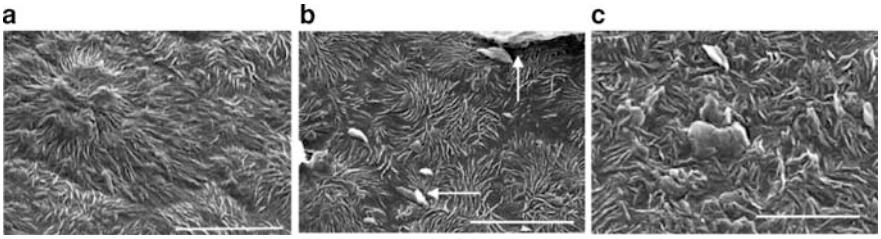

Fig. 7.21 Morphological structures of polyethylene – MMT composites (Vaughan et al. 2006):
(**a**) normal spherulitic structure for unfilled PE (scale bar = 10 μm).
(**b**) Poor dispersal – bright inclusions are aggregates of MMT (scale bar = 10 μm).
(**c**) Well dispersed MMT – morphology is highly perturbed by MMT (scale bar = 5 μm)

Figure 7.21a shows a SEM image of an etched surface of unfilled PE in which the banded spherulites can be clearly seen. Figure 7.21b shows a 5% addition of MMT in which there is poor dispersion. There is no evidence of the polyethylene interacting with the MMT: the spherulitic structure is very similar to Fig. 7.21a and aggregates of MMT are clearly seen to exist. In Fig. 7.21c, in which the workers had set out to disperse the MMT maximally, although aggregates can still be seen, it is generally difficult to distinguish the MMT platelets from the polymer lamellae. The morphology has been grossly disturbed and there is now little evidence of spherulitic structure. This has made a huge difference to the breakdown voltage. Figure 7.22 shows Weibull plots for the poorly dispersed and well dispersed materials corresponding to Fig. 7.21b, c. The better dispersed material, with the much more irregular lamella structure, results in a higher breakdown strength (an increase in the α value from ∼120 to ∼180 kV/mm) and an increase in β from ∼10 to ∼20.

Figure 7.23 depicts the results of Hoyos et al. (2008), who found similar results using a variety of MMT formulations with LDPE. The reader is referred to the original paper for details. They were able to achieve extremely high β values of >70 (i.e., extremely reproducible results) indicating that the effect of the nano-additive had produced a material that was highly uniform and homogeneous. The characteristic breakdown voltage (α), defined by (A.12), increased slightly but the increase in β is highly significant if high reliability systems are to be produced. They considered that a laminar geometry "is a must" if an increase in dielectric strength is required. They also note that adequate processing conditions are required for increasing the value of the shape parameter.

7.3.3 Epoxy Nanocomposites

Montanari et al. (2005) using nanostructured epoxy-silicate insulating materials found similar results. They concluded that the characteristic breakdown voltage was not changed by nanostructuring the material (it remained at 31.1 kV/mm) but that

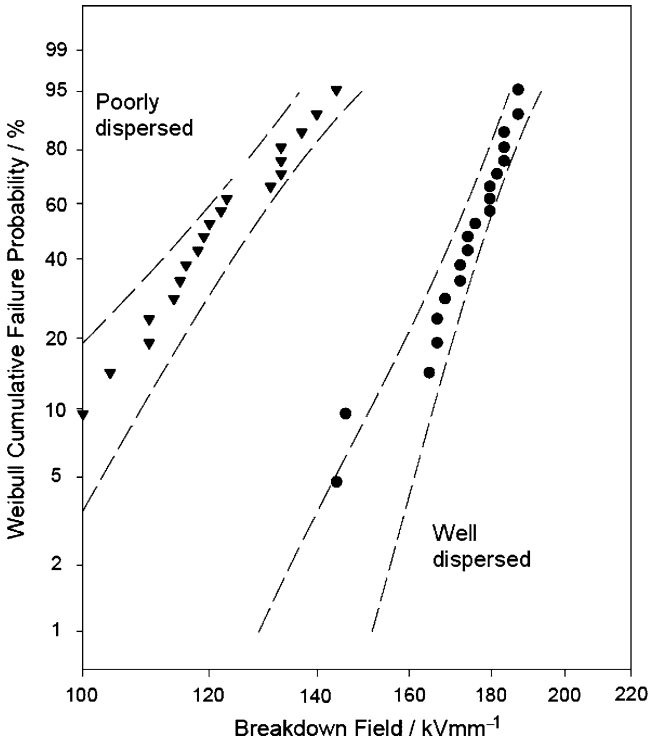

Fig. 7.22 Breakdown voltage of polyethylene – MMT composites (Vaughan et al. 2006)

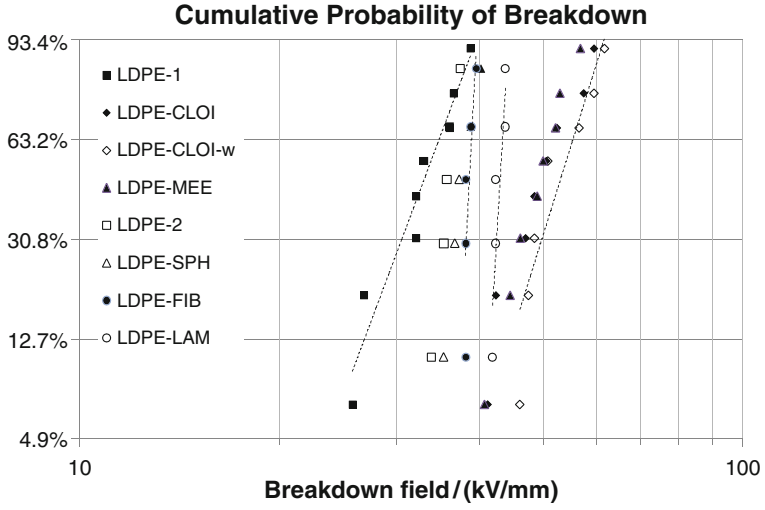

Fig. 7.23 LDPE-MMT nanocomposites formulated by Hoyos et al. (2008). The LDPE-LAM curve has a β value >70

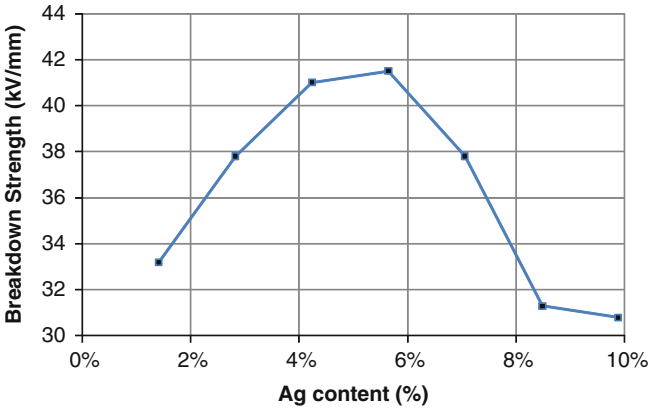

Fig. 7.24 AC breakdown strength of nano-Ag – epoxy resin composites

the shape parameter increased from 60 to 112. This was attributed to a more homogeneous material and, they speculate, that the nanocomposite may have fewer microcavities.

It is interesting that even conducting nanoparticles may lead to an increase in breakdown strength. Wang et al. (2006) have measured the AC breakdown strength of nano-silver – epoxy resins and find an increase in breakdown strength as shown in Fig. 7.24. They invoke a "coulomb blockade" mechanism to explain this phenomenon. The results also show another common effect: if the loadings of nanoparticles exceed a certain amount, the dielectric breakdown strength starts to reduce again. This has been reported by Nelson et al. (2003) who found a loading of about 5% to be optimum for some epoxy–ceramic nanocomposites.

7.3.4 PVA Nanocomposite

Tuncer et al. (2007) investigated the dielectric properties (as a function of frequency and temperature), and the conduction and breakdown properties of a nanocomposite comprising poly-vinyl-acetate (PVA) with barium titanate. The breakdown results obtained from a short-term ramp test are shown in Fig. 7.25. Again the Weibull shape parameter appears to have increased more than the value of characteristic breakdown strength.

7.3.5 Surface Functionalization of Nanoparticles

The results of the above suggest that "nanomization" would tend to improve the reliability of dielectrics by increasing the shape parameter rather than increasing the characteristic breakdown strength. Increases in the shape parameter suggest an

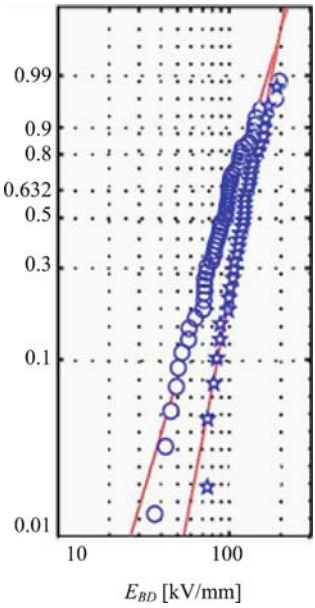

Fig. 7.25 Short-term breakdown test on a PVA – barium titanate nanocomposite. *Circles* = unfilled PVA, *stars* = 6.9 wt% filled PVA (Tuncer et al. 2007)

increased homogeneity on the scale that is important to breakdown – this may be the result of decreasing the concentration or size of micro-cavities that are likely to precipitate breakdown.

However, Roy et al. (2008) (as well as others) have shown that appropriate surface functionalisation may also increase the breakdown strength – without adversely affecting the shape parameter. In this work, the DC breakdown strength was measured using recessed specimens with gold electrodes with specimens ranging in thickness from 0.15 to 0.015 mm. The recessed samples were created using a mold that allowed 25 samples to be prepared on a single wafer thereby allowing multiple specimens to be created simultaneously to permit the large number of breakdown measurements needed to obtain reliable estimates of stochastic parameters. Their results have been shown earlier in Fig. 1.8 and certainly appear to show that surface functionalization is capable of increasing the characteristic breakdown strength, α. The results of this work were obtained for several temperatures. For example, at 25°C, the vinylsilane ("TES") treated nanosilica composites had α (kV/mm) and (β) values of 446 and (1.73) compared with 269 and (2.49) for unfilled XLPE.

7.3.6 Voltage Endurance

Roy et al. (2008) have also reviewed work on *voltage endurance*, i.e., the time-to-breakdown upon the application of a given field. Their results, Fig. 7.26, are relating to the highly divergent fields that occur from electrode pin tips. The fields are therefore much higher than those found in most engineering applications. Their results may relate to electrical tree growth rather than long term aging mechanisms. The re-

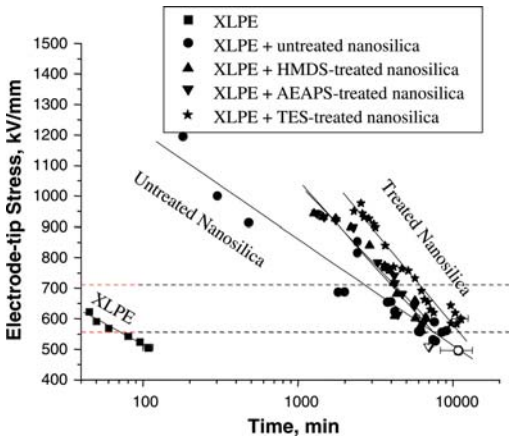

Fig. 7.26 Voltage endurance of XLPE and untreated and functionalized nanocomposites (Roy et al. 2007)

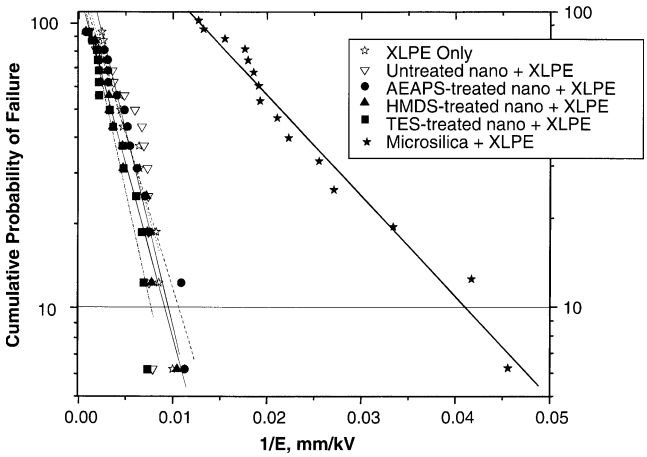

Fig. 7.27 Failure probability as a function of reciprocal field (Roy et al. 2007)

sults indicate the massive improvements that show how important this work is. Gone are the days of incremental improvements in this area; this is a major step forward.

Comparing nanocomposites with micro-composites, it is obvious that nanocomposites are more likely to be uniform than micro-composites. Generally micro-composites contain much higher levels of fillers and it would not be surprising if there were voids surrounding the crevices in such materials. In nanocomposites, although there could conceivably be voids and crevices, these would be on much smaller scales and unlikely to lead to breakdown. If one assumes that the size of defects is exponentially distributed and that the breakdown strength is inversely proportional to the size of the defect then Roy et al. (2007) point out that it is possible to plot the cumulative probability of failure as a function of 1/E to test this hypothesis. Figure 7.27 shows the results represented previously in Fig. 1.8 in this way. This suggests that the micro-composite must have a much larger defect size distribution that the nanocomposites and the base polymer.

7.4 Concluding Comments

Including nanoparticles in insulating polymers has significant effects on the electrical charge transport, dielectric breakdown and endurance properties of materials. To understand these, it is necessary to consider both how the particles change the morphology and local chemistry and physical structure of the polymer. It is also necessary to consider how electrostatic forces around the particle surfaces, resulting in an interaction zone, change the electrical properties.

Nanocomposites appear to increase the DC dielectric breakdown strength and voltage endurance in comparison to unfilled and micron filled materials. The increase in the shape parameter for layered composites suggests that the materials are more homogeneous at the scales relevant for causing breakdown. If one assumes that this may be due to discharges, then this scale may be of the 100s of nm. It has been shown that nanoparticles certainly interfere with the morphology of polyethylene, for example. The particles may also act as "scattering centers" preventing gaseous discharges from taking place but also preventing solid-state avalanches. In either case, the nanoparticles would prevent the carrier multiplication normally recognized as being necessary for breakdown to occur.

Surface functionalisation, whilst important, does not lead to such significant effects as the inclusion of nanoparticles. It is also unclear how such functionalization would affect the interaction zones and hence the electrical transport properties and the mitigation of space charge. However, it is important in controlling the morphological structure of the surrounding polymer. Lewis stated in his 1994 paper, "It has been shown that the dielectric and conductive properties of interfaces will be important if, as seems inevitable, dielectric materials are to be incorporated in nanometric scale devices. ... Equally important will be applications of these interfacial ideas to the technical problem of the electrical breakdown of solid and liquid insulants." How right he was!

References

Balberg I (2009) Tunnelling and percolation in lattices and the continuum. J Phys D Appl Phys 42:1848–1852

Bertini GJ (2009) Diagnostic testing of stochastic cables. IEEE Electr Insul Mag 25(2):6–12

Cao Y, Irwin PC (2003) The electrical conduction in polyimide nanocomposites. IEEE Conf Electr Insul Dielectr Phenom: 116–119

Cao Y, Irwin PC, Younsi K (2004) The future of nanodielectrics in the electrical power industry. Trans IEEE DEI-11(5):797–807

Chutia J, Barua K (1980) DC conduction phenomenon in polyvinylacetate films. J Phys D Appl Phys 13:L9–L13

Dissado L A, Hill R M (1984) Anomalous low frequency dispersion. A near DC conductivity in disordered low dimensional materials. J Chem Soc Faraday Trans II 80:291–319

Dissado LA, Hill RM (1988) Constant-phase-angle and power-law regimes in the frequency response of a general determinate fractal circuit. Phys Rev B 37:3434–3439

Dissado LA and Fothergill JC (1992) Electrical degradation and breakdown in polymers. Peter Peregrinus Ltd. for the IEE, London

Elmahdy MM, Chrissopoulou K, Afratis A et al (2006) Effect of confinement on polymer segmental motion and ion mobility in PEO/layered silicate nanocomposites. Macromolecules 39(16):5170–5173

Fothergill JC (2007) Ageing, space charge and nanodielectrics: ten things we don't know about dielectrics, IEEE Int Conf Solid Dielectr: 1–10

Grosse C (2006) Dielectric properties of suspensions of solid particles. In: Encyclopedia of surface and colloid science. Taylor and Francis, 1688–1705

Hayase Y, Aoyama H, Tanaka Y et al (2007) Space charge formation in LDPE/MgO nanocomposite thin film under ultra-high DC electric stress. Proc IEEE Int Conf Prop Appl Dielectr Mater: 159–162

He D, Ekere NN (2004) Effect of particle size ratio on the conducting percolation threshold of granular conductive – insulating composites. J Phys D Appl Phys 37:1848–1852

Holé S, Sylvestre A, Gallot Lavellée O et al (2006) Space charge distribution measurement methods and particle loaded insulating materials. J Phys D Appl Phys 39:950–956

Hoyos M, Garcia N, Navarro R et al (2008) Electrical strength in ramp voltage AC tests of LDPE and its nanocomposites with silica and fibrous and laminar silicates. J Polym Sci B 46(13):1301–1311

IEEE Standard 930-2004 (2004) IEEE guide for the statistical analysis of electrical insulation breakdown data, ISBN 0-7381-4468-1 SH95269

Jonscher AK (1983) Dielectric relaxation in solids. Chelsea Dielectric Press, London, Section 5.6

Lampert MA, Mark P (eds) (1970) Current injection in solids, Academic, New York p 24

Lewis TJ (1954) The work function of irregular metal surfaces. Proc Phys Soc B 67(3):187–200

Lewis TJ (1994) Nanometric dielectrics. Trans IEEE DEI-1(5):812–825

Lewis TJ (2004) Interfaces are the dominant feature of dielectrics at the nanometric level. Trans IEEE DEI-11(5):739–753

Ma D, Hugener TA, Siegel RW et al (2005) Influence of nanoparticle surface modification on the electrical behavior of polyethylene nanocomposites. Nanotechnology 16(6):724–731

Montanani GC, Ciani F, Testa L et al (2005) Electric strength, space charge and surface discharge characterization of nanostructured epoxy-silicate insulating materials. Int Symp Electr Insul Mater 206–209

Mott MF and Gurney RW (1940) Electronic processes in ionic crystals. Oxford University Press, London

Mott MF (1967) Electrons in disordered structures. Adv Phys 16(61):49–144

Murata Y, Goshowaki M, Reddy CC (2008) Investigation of space charge distribution and volume resistivity of XLPE/MgO nanocomposite material under DC voltage application. IEEE Int Symp Electr Insul Mater: 502–505

Nelson JK, Fothergill JC, Dissado LA, Peasgood W (2002) Towards an understanding of nanometric dielectrics. IEEE Conf Electr Insul Dielectr Phenom: 295–298

Nelson JK, Hu Y, Thiticharoenpong J (2003) Electrical properties of TiO_2 nanocomposites. IEEE Conf Electr Insul Dielectr Phenom: 295–298

Nelson JK, Fothergill JC (2004) Internal charge behavior of nanocomposites. Nanotechnology 15:1–10

Peacock A (2000) Handbook of polyethylene structures, properties and applications. CRC, Boca Raton, FL

Roy M, Nelson JK, MacCrone RK, Schadler LS (2007) Candidate mechanisms controlling the electrical characteristics of silica/XLPE nanodielectrics. J Mater Sci 42:3789–3799

Teyssedre G, Laurent C, Montanari GC et al (2001) Charge distribution and electroluminescence in cross-linked polyethylene under dc field. J Phys D 34(18):2830–2844

Tanaka T, Montanari GC, Mülhaupt RM (2004) Polymer Nanocomposites as dielectrics and electrical insulation – Perspectives for processing technologies, material characterization and future applications. Trans IEEE DEI-11(5):763–784

Tuncer E, Duckworth RC, Sauers I (2007) Dielectric properties of polyvinyl alcohol filled with nanometer size barium titanate particles. IEEE Conf Electr Insul Dielectr Phenom: 225–227

Vaughan AS, Swingler SG, Zhang Y (2006) Polyethylene nanodielectrics: the influence of nanoclays on structure formation and dielectric breakdown. IEEJ Trans Fundam Mater 126(11):1057–1063

Wang L, Xu M, Feng J, Cao X (2006) Study on AC breakdown property of nanoAg/epoxy resin composite. IEEE Int Conf Prop Appl Dielectr Mater 163–166

Wintle HJ (1983) Conduction processes in polymers. In: Bartnikas R, Eichorn RM (eds). Engineering dielectrics. Vol IIA, Electrical properties of solid insulating materials: molecular structure and electrical behaviour. ASTM Special Technical Publication 783, Philadelphia, PA 239–354

Zilg C, Kaempfer D, Thotnann R (2003) Electrical properties of polymer nanocomposites based upon organophilic layered silicates. IEEE Conf Electr Insul Dielectr Phenom: 546–550

Zhang P, Li G, Gai L, Lei Q (2006) Conduction current characteristics of nanoinorganic composite polyimide films. Proc IEEE Int Conf Prop Appl Dielectr Mater: 755–758

Zou C, Fothergill JC, Rowe SW (2008) The effect of water absorption on the dielectric properties of epoxy nanocomposites. Trans IEEE DEI-15(1):106–117